Charge injection enhanced natural convection heat transfer in horizontal concentric annuli filled with a dielectric liquid

Jian Wu[a1], Philippe Traoré[a], Mengqi Zhang[a], Alberto T. Pérez[b], Pedro A. Vázquez[c]

[a] Institut PPRIME, Département Fluide-Thermique-Combustion, Université de Poitiers, Boulevard Pierre et Marie Curie, BP 30179, 86962 Futuroscope-Chasseneuil, France

[b] Departamento de Electrónica y Electromagnetismo, Universidad de Sevilla, Facultad de Física, Avenida Reina Mercedes s/n, 41012 Sevilla, Spain n

[c] Departamento de Física Aplicada III, Universidad de Sevilla, ESI, Camino de los Descubrimientos s/n, 41092 Sevilla, Spain

Abstract

The natural convection heat transfer in a highly insulating liquid contained between two horizontal concentric cylinders is shown by two-dimensional numerical simulations to be noticeably enhanced by imposing a direct current electric field. This augmentation of heat transfer is due to the radial flow motion induced by unipolar injection of ions. It is found that there exists a threshold of the electric driving parameter *T*, above which the heat transfer enhancement due to the electric effect becomes significant. For relatively small *T* values, the mean Nusselt numbers are closely related to the flow pattern and Rayleigh number *Ra*. In addition, for sufficiently high *T* values, the flow is fully dominated by the Coulomb force, and thus the heat transfer rate no long depends on *Ra*.

Keywords: Electrohydrodynamics; heat transfer enhancement; charge injection; concentric annuli; numerical analysis; dielectric liquids

[1]Corresponding author. E-mail address: jian.wu@univ-poitiers.fr and xikuanghit@gmail.com (Jian Wu).

1. Introduction

Electro-Thermo-Hydro-Dynamics (ETHD) is an interdisciplinary field involving complex interactions among the fluid motion, the thermal field and electrostatics [1,2]. The active augmentation of convective heat transfer by electrical forces is an important application in this field. Indeed, there are some unique advantages for heat transfer enhancement due to the electrical effect, such as the simple design, rapid and smart control of enhancement, no need of mechanical parts, low power consumption, and so on [3]. The earliest work on this subject may date back to the mid-1930s when Senftleben and Braun performed experiments of heat transfer enhancement due to the electric field in gases [4]. In the early 1950s, the first results of the influence of electric fields on convective heat transfer in dielectric liquids were reported [5,6]. Some recent experimental studies include the heat transfer augmentation using corona jets [7] and ionic winds [8], and by means of electrohydrodynamic (EHD) conduction pumping [9] and ion injection from a sharp metallic electrode in dielectric liquids [10], etc. Besides [1,3], there are several state-of-the-art reviews that cover different aspects of electrohydrodynamical enhancement of heat transfer [11,12,13].

In general, when a dielectric liquid is subjected to an external electric field, the electrical body force $\vec{f}_E$ arises and it may be expressed as,

$$\vec{f}_E = q\vec{E} - \frac{1}{2}E^2\nabla\varepsilon + \frac{1}{2}\nabla\left[\rho E^2\left(\frac{\partial\varepsilon}{\partial\rho}\right)_\theta\right] \tag{1}$$

where q denotes the free charge density, $\vec{E}$ the electric field, ε the dielectric permittivity, ρ the fluid density, and θ the absolute temperature. The three terms on the right-hand side of Eqn. (1) represent the Coulomb force on free charges, the dielectric force and the electrostritive force, respectively. The electrostritive force can be incorporated into the pressure term since it can be

viewed as the gradient of a scalar field, and thus it will not affect the single-phase flow [14]. The dielectric force requires a non-zero permittivity gradient, which may be achieved by imposing a temperature gradient and at the same time assuming that the permittivity is temperature-dependent [15]. However, under a direct current (DC) electric field, it is generally much weaker than the Coulomb force when there are non-negligible space charges within the liquid [14]. It should be noted that the dielectric force may become dominant (or even the only electrical body force) when an alternating current (AC) field is applied (see for example refs. [16,17,18,19,20]). The Coulomb force refers to the force exerted by the electric field on the free charges present in the liquid. It is commonly the strongest electrical force when a DC field is applied [14,21].

To better understand the mechanism of the heat transfer enhancement by EHD, it is necessary to discuss the generation of the free space charges in the flow. Various physical mechanisms have been proposed to account for the originations of free space charges. Some studies considered charges resulting from a thermally induced conductivity gradient within the liquid (see for example refs. [22,23,24]). However, this model fails to explain the nonlinear current-voltage (I-V) characteristics of dielectric liquids for strong electric fields ($E > 10^4$ V/m) [14] and also the electro-convection observed in an isothermal dielectric liquid [25,26]. The dissociation-injection conductivity model that takes into account the ion injection at the liquid/electrode interface and the field-enhanced dissociation of impurities (usually salts) in the bulk is able to interpret the I-V characteristics of both highly and weakly insulting liquids for a wide range of the strength of the electric field [27,28,29]. When an intense electric field is applied to a highly insulating liquid, the injection of ions, which occurs at the electrical double layer due to electrochemical reactions, is considered as the main source of free charges [30]. Both theoretical analysis and experimental results have shown that the reproducible ion injections can be achieved by adding some salt into

an insulating liquid [30,31]. It should be noted that though the added salt can facilitate the charge injection, it also results in a non-negligible residual conductivity.

The material presented here represents the first results of a broader research project aimed at numerically studying injection-dissociation enhanced convection heat transfer in dielectric liquids for practical applications. Previous studies based on a similar or the same physical model mainly focused on the linear instability feature of the problem [2,32]. In addition, most of these studies dealt with the simplest plate-plate configuration. From a practical point of view, the configurations of complex geometries, such as concentric and eccentric cylinders, blade/point-plate, etc., are more interesting. Two straightforward examples of application are the forced flows in pipes (wire/cylinder) [33] and fluid-filled underground electric transmission cables [34]. In this study, we consider injection as the sole source of free charges and the injection-induced secondary flows to enhance natural convection heat transfer in a horizontal concentric annulus. The present study may be viewed as an extension of our recent work on electro-thermo-convection in a planar layer of dielectric liquid [35,36]. As will be shown later, the change in geometry leads to some interesting phenomena. In another recent study [37], we numerically studied the annular electro-convection in an isothermal liquid induced by a strong unipolar injection between two coaxial cylinders, which can be viewed as the up-front work.

The remainder of this paper is organized as follows. In the next section, the physical problem is described and the mathematical model and boundary conditions are stated. Then we make a brief description of the numerical method in section 3. In section 4, numerical results are presented and discussed. Finally, in section 5, we summarize our findings and point out some subsequent working directions.

2. Physical problem and mathematical formulation

The physical configuration and the two-dimensional Cartesian coordinate system (x,y) used in this work is sketched in Fig. 1. We consider an incompressible Newtonian dielectric liquid contained between two infinitely long horizontal concentric cylinders, of which the inner and outer radii are denoted by R_i and R_o, respectively. A radial DC electric field is applied across the liquid layer. The inner cylinder is kept at a constant potential V_0 (> 0) while the outer cylinder is grounded, i.e., $V_1 = 0$. The inner and outer cylinders are maintained at uniform but different temperatures, θ_h and θ_c ($\theta_h > \theta_c$), respectively. The liquid is assumed to be highly insulating, and thus all free charges are from the unipolar injection-process at the inner cylinder. To further simplify the discussion, the injection is assumed to be *autonomous* and *homogeneous*. That is, the injected charge density at the emitter electrode is uniform and takes a constant value q_0. This autonomous injection can be viewed the limiting case of a general injection law proposed in [31], and it works well for a wide range of strong electric field. In addition, we assume that the charge carriers are instantaneously discharged once they arrive at the outer cylinder.

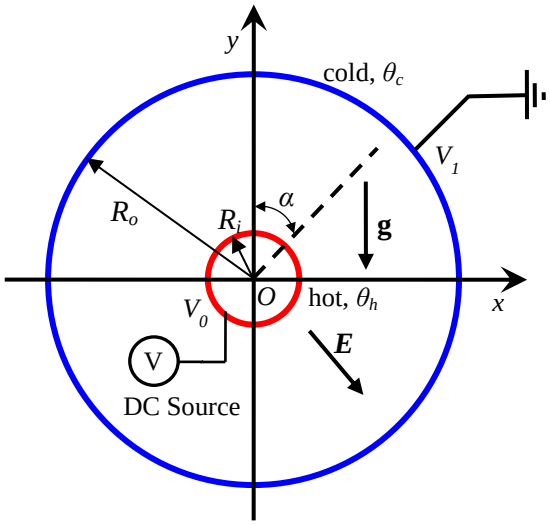

FIG.1. A dielectric liquid layer lying between two concentric cylinder electrodes and subjected to an applied DC voltage and a thermal gradient.

Let ρ be the density of the fluid, ν the kinematic viscosity, c_p the specific heat at constant pressure, κ the thermal diffusivity, and ε the dielectric permittivity. Under the Oberbeck-Boussinesq approximation, the flow is governed by the equation of continuity,

$$\nabla \cdot \vec{U} = 0, \tag{2}$$

the Navier-Stokes equations including the electrical force and the buoyancy force,

$$\rho_0 \left(\frac{\partial \vec{U}}{\partial t} + \vec{U} \cdot \nabla \vec{U} \right) = -\nabla p + \rho_0 \nu \nabla^2 \vec{U} + \vec{f}_E - \rho \vec{g}, \tag{3}$$

the energy equation,

$$\frac{\partial \theta}{\partial t} + \vec{U} \cdot \nabla \theta = k \nabla^2 \theta, \tag{4}$$

the charge density transport equation and Gauss' law for the electric field,

$$\nabla \cdot \left(\varepsilon \vec{E} \right) = q, \tag{5}$$

$$\vec{E} = -\nabla V, \tag{6}$$

$$\frac{\partial q}{\partial t} + \nabla \cdot \left(qK\vec{E} + q\vec{U} - D\nabla q \right) = 0, \tag{7}$$

together with the state equation for the fluid density,

$$\rho = \rho_0 \left[1 - \beta \left(\theta - \theta_0 \right) \right]. \tag{8}$$

The vectors $\vec{U} = [u, v]$, $\vec{E} = [E_x, E_y]$, $\vec{g} = -g\vec{e}_y$ $(g > 0)$ and $\vec{e}_y$ denote the fluid velocity field, electric field, gravitational acceleration, and the unit vector in the positive y-direction. The scalars p, q, V and θ stand for the dynamic pressure, charge density, electric potential and temperature. K denotes the ionic mobility and D is the charge diffusion coefficient. ρ_0 is the density defined at the reference value of temperature, θ_0 (here $\theta_0 \equiv \theta_c$). The coefficient β denotes the derivative of ρ / ρ_0 with respect to temperature. For highly insulating fluids, the

electric current through the dielectric liquid is generally weak, thus the magnetic effects and the Joule heating are neglected. In addition, the dielectric permittivity ε and the ionic mobility K are assumed to be constant. As a result, the dielectric force vanishes. The above mathematical model has been extensively used in modelling of electro-thermo-hydrodynmic flow [2,27].

To work in the dimensionless form, the following transformations are made for length, liquid velocity, time, pressure, electric potential, electric field, charge density, temperature and fluid density,

$$[x,y]=[x',y']\cdot H,\qquad \overset{\mathrm{v}}{U}=\overset{\mathrm{v}}{U}'\frac{\nu}{H},\qquad t=t'\frac{H^2}{\nu},\qquad p=p'\frac{\rho_0\nu^2}{H^2},\qquad V=V'V_0,$$

$$\overset{\mathrm{v}}{E}=\overset{\mathrm{v}}{E}'\frac{V_0}{H},\qquad q=q'q_0,\qquad \theta=\theta_c+\theta'(\theta_h-\theta_c),\qquad \rho=\rho'\rho_0,$$

where $H=R_o-R_i$ and quantities with prime are non-dimensional. The resulting non-dimensional equations are (for clarity, we omit the prime in the equations below),

$$\nabla\cdot\overset{\mathrm{v}}{U}=0, \tag{9}$$

$$\frac{\partial\overset{\mathrm{v}}{U}}{\partial t}+\left(\overset{\mathrm{v}}{U}\cdot\nabla\right)\overset{\mathrm{v}}{U}=-\nabla\hat{p}+\nabla^2\overset{\mathrm{v}}{U}+\frac{T^2}{M^2}qC\overset{\mathrm{v}}{E}+\frac{Ra}{Pr}\theta\overset{\mathrm{v}}{e}_y, \tag{10}$$

$$\frac{\partial\theta}{\partial t}+\overset{\mathrm{v}}{U}\cdot\nabla\theta=\frac{1}{Pr}\nabla^2\theta, \tag{11}$$

$$\frac{\partial q}{\partial t}+\nabla\cdot\left[\left(\frac{T}{M^2}\overset{\mathrm{v}}{E}+\overset{\mathrm{v}}{U}\right)q\right]=\hat{D}\nabla^2q \tag{12}$$

$$\nabla^2V=-Cq, \tag{13}$$

$$\overset{\mathrm{v}}{E}=-\nabla V, \tag{14}$$

where $\hat{p}$ is the modified pressure including an extra component from the electrostrictive force [14]. Six dimensionless numbers defined as follows appear,

$$Ra=\frac{g\beta\Delta\theta H^3}{\kappa\nu},\quad Pr=\frac{\nu}{\kappa},\quad T=\frac{\varepsilon\Delta V}{\rho\nu K},\quad C=\frac{q_0H^2}{\varepsilon\Delta V},\quad M=\frac{1}{K}\left(\frac{\varepsilon}{\rho}\right)^{1/2},\quad \hat{D}=\frac{D}{\nu}.$$

Ra and *Pr* are the Rayleigh number and the Prandtl number. The electric Rayleigh number *T* is defined as the ratio between the Coulomb force and the viscous force, and it can be viewed as a dimensionless representative of the applied voltage. The injection strength number *C* is a measure of how the injected charge influences the electric field distribution. For *C* much less than one the electric field is given by the solution of Laplace equation, and for *C* much greater than one the electric field is greatly modified by the presence of the space charge, being almost zero at the injector. *M* is the dimensionless mobility number, defined as the ratio between the so-named hydrodynamic mobility and the true ionic mobility. Both *Pr* and *M* are decided by the fluid properties. $\hat{D}$ is the dimensionless charge diffusion coefficient. Since typical values for $\hat{D}$ with dielectric liquids are in the range between 10^{-4} and 10^{-3} [38], the charge conservation equation (12) is strongly convection-dominating. In addition, the problem also depends on the geometry of the concentric annulus, so we define the radius ratio Γ as $\Gamma=R_i/R_o$, ($0<\Gamma<1$).

To quantitatively evaluate the enhancement in heat transfer, the local Nusselt numbers defined at the inner and outer cylinders are computed as,

$$Nu_i=R_i\ln\left(\frac{R_o}{R_i}\right)\left.\frac{\partial\theta}{\partial r}\right|_{r=R_i}\quad\text{and}\quad Nu_o=R_o\ln\left(\frac{R_o}{R_i}\right)\left.\frac{\partial\theta}{\partial r}\right|_{r=R_o},\tag{14}$$

where $\partial\theta/\partial r$ is the temperature gradient in the radial direction. The mean Nusselt number is computed as,

$$\overline{Nu}=\frac{1}{2}\left(\overline{Nu}_i+\overline{Nu}_o\right)=\frac{1}{2}\left(\frac{1}{2\pi}\int_0^{2\pi}Nu_i(\alpha)d\alpha+\frac{1}{2\pi}\int_0^{2\pi}Nu_o(\alpha)d\alpha\right)\tag{15}$$

where α denotes the angle, see Fig. 1.

The computational domain is defined by the annulus of $R_i = \Gamma/(1-\Gamma) \le r \le 1/(1-\Gamma) = R_o$ and $0 \le \alpha < 2\pi$. The associated boundary conditions are summarized as,

inner cylinder (hot injector), $r = R_i$: $u = v = 0$, $\theta = 1$, $V = 1$, $q = 1$;

outer cylinder (cold collector), $r = R_o$: $u = v = 0$, $\theta = 0$, $V = 0$, $\partial q/\partial r = 0$;

which means that the no-slip conditions for fluid are imposed at impermeable, thermally and electrically perfectly conducting electrodes.

3. Computational technique

The numerical algorithm we proposed in [36] for electro-thermo-convection between two parallel plates has been extended here to the configuration of concentric cylinders. A numerical solver based on a 2nd order finite volume method is used to solve Eqns. (9)-(14) in the primitive variables (u, v, θ, V, q) [39]. The computational domain is discretized with a boundary-fitted structured grid with orthogonal quadrilateral meshes. All variables are stored at the center of each control volume (i.e., a colocated arrangement). Figure 2 shows an example of discretized grid. The grid is uniform in the azimuthal direction and non-uniform in the radial direction. The finer grid size in the region close to the emitter cylinder aims at capturing the sharp variation in the charge density distribution within this region.

For the Navier-Stokes equations, the central differencing (CD) scheme is used to compute the convective flux. Since the grid is non-orthogonal, we employed the over-relaxed approach [40,41] to take into account the non-orthogonal component of the diffusive flux. The time integration was performed by the semi-implicit three time levels scheme [39]. The SIMPLE algorithm [42] and Rhie-Chow scheme [43] are employed for velocity-pressure coupling and momentum interpolation, respectively. A detailed description of the algorithm for the energy equation (11) and electrostatic equations (12-14) is provided in [44]. In particular, the Smooth Monotonic

Algorithm for Real Transport (SMART) scheme of Gaskell & Lau [45] is applied to the convection-dominating equation (12), aiming at preventing unphysical oscillations and simultaneously reducing the numerical diffusion. For more details with the overall solution procedure and the description of the nonlinear couplings among different fields, we refer the interested readers to [36].

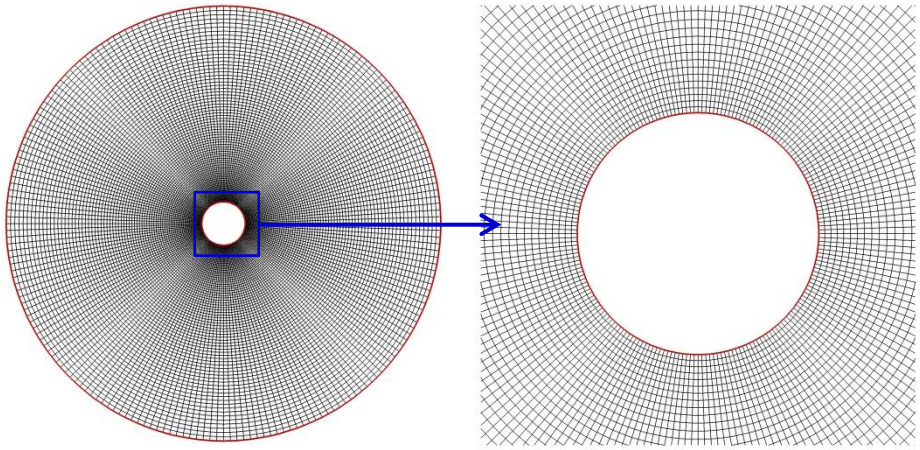

FIG.2. An example of discretized grid consisting of structured quadrilateral meshes.

4. Results and discussion

Computations are carried out for a fixed radius ratio $\Gamma = 0.1$, a strong injection $C = 10$ and for the Rayleigh number range $[0, 2\times10^4]$. This injection value has been extensively used in previous numerical studies, and it can be viwed as a good approximation of the so-named Space-Charge-Limited (SCL) injection, for which can be experimentally achieved by covering the electrode with membrane [25]. The charge diffusion coefficient $\hat{D}$ is also fixed at 5×10^{-4}. A small radius ratio considered here aims to approximate the practical applications using wire as the emitter. The silicon oil used in the experimental studies [46,47] are chosen as the working medium. The relevant physical properties of this liquid can be found in [47], and the corresponding values of Pr and M for this liquid are 116.6 and 49.0, respectively. After the grid independence test, we

finally chose a non-uniform grid with 400×150 cells for all computations. In the following, we first present the results of natural convection (pure thermal convection) and pure electro-convection to validate our numerical solver and to highlight the difference between the two types of basic flows. Then the results of the heat transfer enhancement resulting from charge injection are summarized and discussed.

4.1 Natural convection and pure electro-convection in horizontal concentric annuli

Natural convection between concentric isothermal cylinders is a classical problem in non-isothermal fluid mechanics [48,49,50]. Unlike Rayleigh-Bénard convection of a horizontal fluid layer heated from below, even a very small temperature difference between the two cylinders will cause fluid motion. For the case considered in this study ($\Gamma = 0.1$, $Pr = 116.6$ and $Ra \leq 2\times10^4$), we obtained steady unicellular convection, which is consistent with the prediction of the flow pattern chart proposed in [51]. In Figs. 3(a-c), the isotherms and stream functions are presented for the cases of three Rayleigh numbers. The flow is characterized by two symmetric (with respect to the virtual line $x = 0$), counter-rotating cells visualized in terms of the stream function. As *Ra* increases, the intensity of convection increases and the centres of convection rolls move upwards. For small *Ra*, the flow is in the 'pesudo-conductive' regime since heat is mainly transferred by conduction [49]. As shown in Fig. 3(a), the isotherms resemble quasi-circles and the centre of rotation is very close to the horizontal line $y = 0$. For higher *Ra*, the flow is of boundary layer type [50]. As shown in Figs. 3(b) and (c), a buoyant plume originates at the top of inner cylinder and impinges towards the outer cylinder.

Results of the mean Nusselt numbers with natural convection are listed in Table 1. For validation, the results obtained with the commercial software FLUENT are also provided. The same number of CVs is used in FLUENT. The results obtained with two different methods are in

good agreement with each other. We notice that though as the increase of *Ra* the mean Nusselt numbers $\overline{Nu}$ increases to a certain extent the overall heat transfer is still constrained. We recall that our main objective in this study is to examine how the heat transfer rate changes when an electric field is imposed across the fluid.

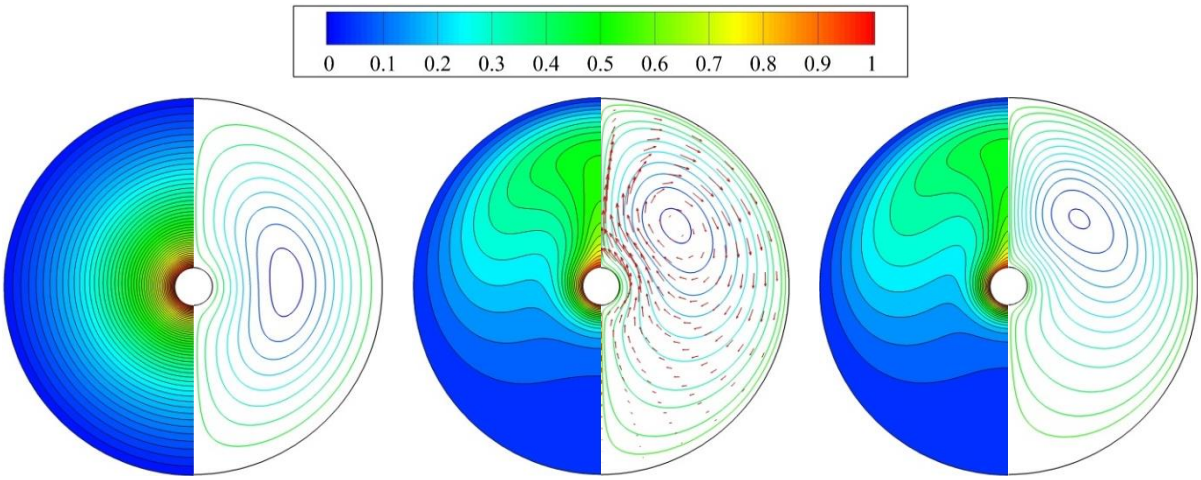

(a) (b) (c)

FIG.3. Temperature isotherms (left half) and stream functions (right half) of natural convection, (a) $Ra = 10^2$, (b) $Ra = 5\times10^3$, (c) $Ra = 2\times10^4$.

Table 1. Mean Nusselt numbers for natural convection, $Pr = 111.6$, $\Gamma = 0.1$.

Ra	10^1	10^2	10^3	5×10^3	10^4	1.5×10^4	2×10^4
$\overline{Nu}$, FVM[a]	1.000	1.001	1.142	1.739	2.035	2.216	2.348
$\overline{Nu}$, FLUENT[b]	1.000	1.001	1.148	1.752	2.059	2.245	2.383

FVM[a], our results with the finite volume method;
FLUENT[b], results from the commercial software FLUENT.

The unipolar injection induced electro-convection in the concentric cylinder configuration is characterized by a hydrodynamic stability [52]. Physically, the flow motion occurs only when the Coulomb force is sufficiently strong to overcome the viscous damping. Otherwise, the fluid remains a rest state and free charges are transported by the migration due to electric field and by molecular diffusion (the hydrostatic state). This linear instability has been well analyzed by the stability analysis approach in several studies [52, 53, 54, 55]. It is found that the stability criterion,

expressed by the electric Rayleigh number T, depends on the injection strength C, the injection direction (inner or outer), the radius ratio Γ, the diffusion coefficient $\hat{D}$, and the form of perturbations (2D or 3D). For the case of (2D, inner injection, C = 10, Γ = 0.1, $\hat{D}$ = 0), we have adopted the same stability analysis method of [52] and determined the critical T value (marked as T_c) and the corresponding mode number (marked as m_c) as 64.11 and 3, respectively.

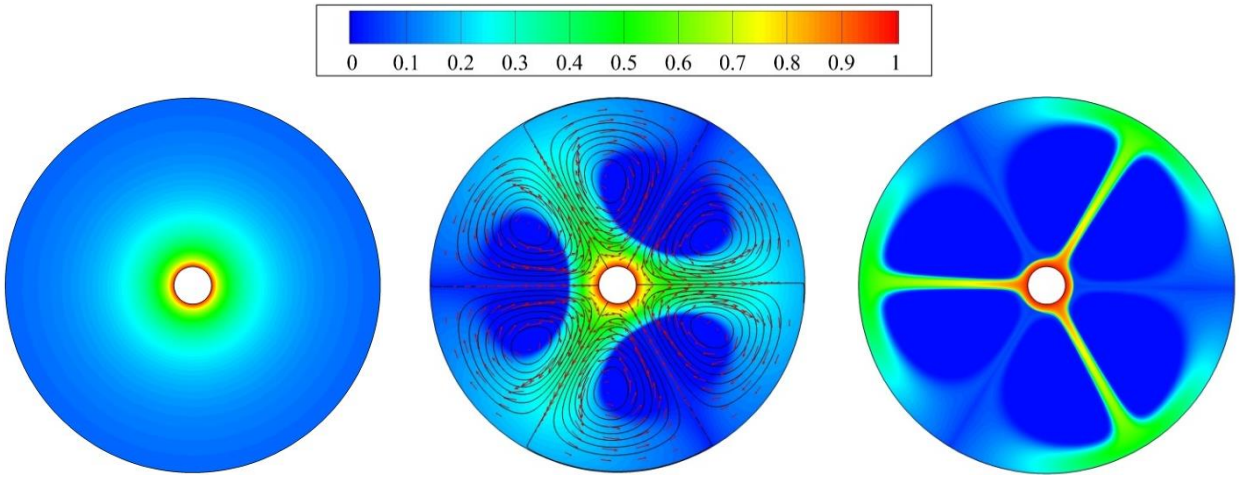

(a) (b) (c)

FIG.4. Charge density distribution and the flow field of pure electro-convection, (a) T = 60, lower than T_c, (b) T = 80, higher than T_c, (c) T = 800. T_c = 64.1, the linear stability criterion.

In Figs. 4a-c, the charge density distributions are presented for three electric Rayleigh numbers. For T=60 < T_c (see Fig. 4a), there is no flow motion, and the charge density distribution follows an analytical expression, $q_s(r) = a/C\sqrt{r^2+b}$ [52], a and b being two constants that depend on C and Γ. For inner injection with C = 10 and Γ = *0.1*, the values of a and b are 1.0090 and −0.0022, respectively [37]. For T = 80, a value slightly higher than T_c (see Fig. 4b), a radial motion with three pairs of counter-rotating cells raises. The number of convective cells is determined by the most unstable mode m_c. Three electro-plumes evenly distribute around the inner cylinder and impinge towards the outer cylinder. In addition, there are three central regions almost free of charges ($q \rightarrow 0$). The charge void region is a characteristic feature of Coulomb-

driven dielectric liquid flows [14]. It is interesting to point out that Fig. 4b share a strong analogy with the electro-convective leaf pattern described in [33]. As the increase of T up to 1000, the charged plumes become thinner and the area of the void region expands; see Fig. 4c. A further increase in T leads to an unsteady flow with the number and positions of electro-plumes continuously changing.

4.2 Heat transfer enhancement due to annular electro-convection

Now we consider how the imposed electric field affects natural convection heat transfer. In each case, the electric field as well as charge injection is applied on a stationary natural convection previously obtained. The charge injection strength C is fixed, while the intensity of electric field is controlled by the electric Rayleigh number T. Our numerical solutions correspond to a two-step experimental process. First, only a temperature difference with its value expressed by Ra is imposed between the two cylinders. After the natural convection reaches a stationary state, a step voltage with its value expressed by T is applied, and then the liquid is under the simultaneous actions of the buoyancy force and the Coulomb force.

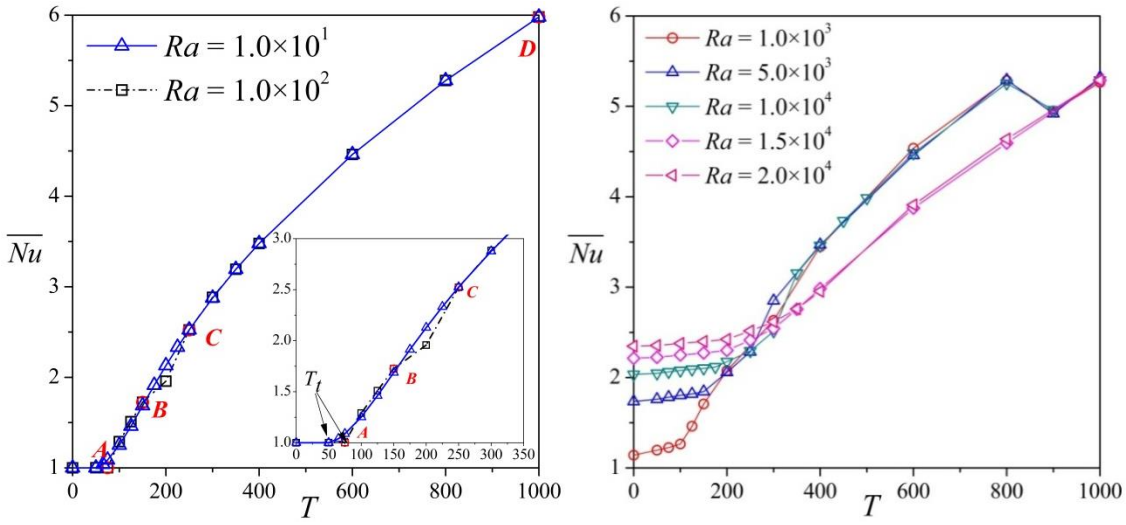

(a) (b)

FIG.5. Mean Nusselt number $\overline{Nu}$ as a function of electric Rayleigh number T for various values of Rayleigh number Ra.

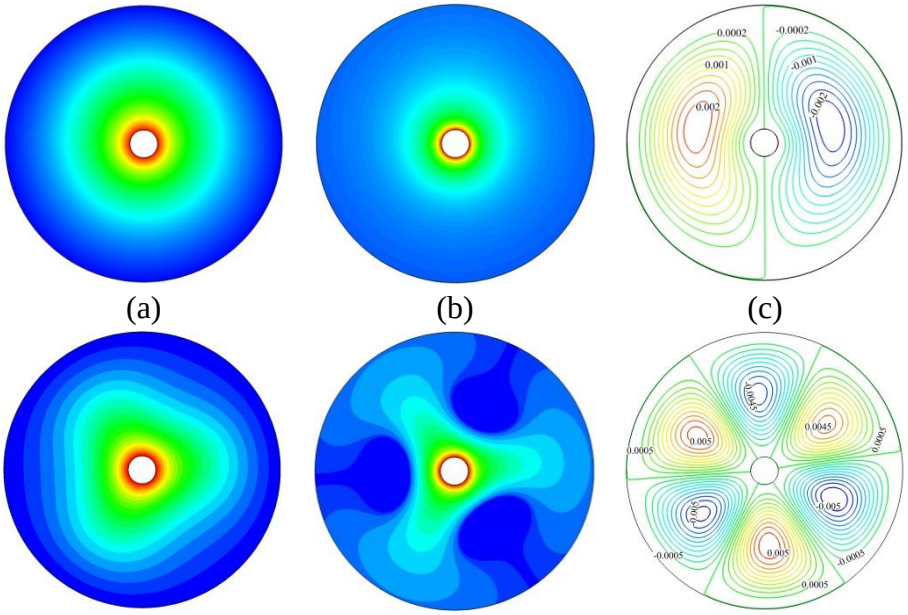

(a) (b) (c)

(d) (e) (f)

FIG.6. Solutions for Ra = 10, T = 60 (top) and 65 (bottom). (a) and (d) - temperature, (b) and (e) - charge density, (c) and (f) - stream function.

Compared to the plate-plate configuration, the electro-thermo-convective phenomena in the cylindrical configuration is much more complex. This is partially due to the differences in the directions of driving forces and also in the basic flow patterns. In Fig. 5 the mean Nusselt numbers $\overline{Nu}$ are plotted against T for various values of Ra investigated. We first notice the existence of a threshold of T (marked by T_t), above which the heat transfer rate rapidly increases along with the increase of T. In the range of $T < T_t$, $\overline{Nu}$ slowly increases with T. In addition, the value of T_t is closely related to Ra. As Ra increases, the value of T_t also increases. For Ra = 10 and 10^2, we find the threshold values are about 65.0 and 75.0, respectively. Both values are close to 64.1, the linear stability criterion of pure electro-convection. For $Ra = 2\times10^4$, the highest Ra value we considered, T_t lies in the range of (200, 250). By checking the flow fields, we find that the radial motion arises only when $T > T_t$. These radial motions usually exhibit more convective

cells, and as a consequence heat transfer rate is higher. The change in the flow pattern when T crosses T_t accounts for the sudden jump of $\overline{Nu}$ at T_t in Fig. 5.

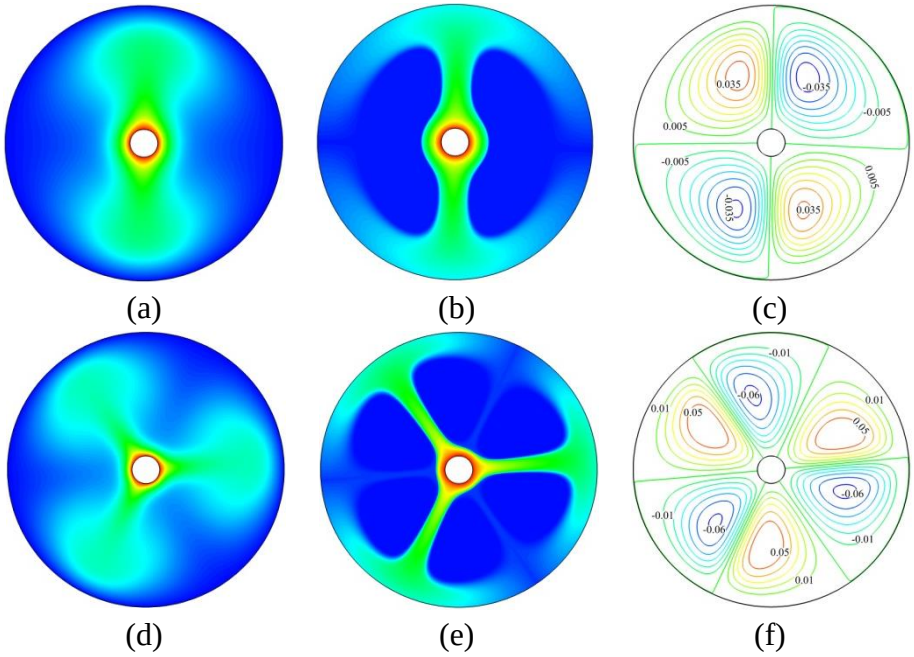

FIG.7. Solutions for $Ra = 10^2$, $T = 150$ (top) and 250 (bottom). (a) and (d) - temperature; (b) and (e) - charge density; (c) and (f) - stream function.

To study how the electric field affects the heat transfer, we first consider the limiting situation that the buoyancy force is weak. In Fig. 6 we have provided two representative examples to show the change of the flow pattern when T crosses T_t. For $T < T_t$, as it can be seen from Fig. 6c, the flow possesses two counter-rotating cells, same as natural convection. Since the strength of motion is too weak, the distributions of temperature and charge density are essentially determined by heat conduction and ion drift, respectively; see Figs. 6a and 6b. Once $T > T_t$, as shown in Figs. 6e and 6f, three pairs of radial cells together with the charge void regions appear, same as pure electro-convection. In this case, the temperature distribution shown in Fig. 6d is determined by the combination of heat conduction and the radial convection. The increase in the number of convective cells results in a higher heat transfer rate and a sudden transition in $\overline{Nu}$ - T curve.

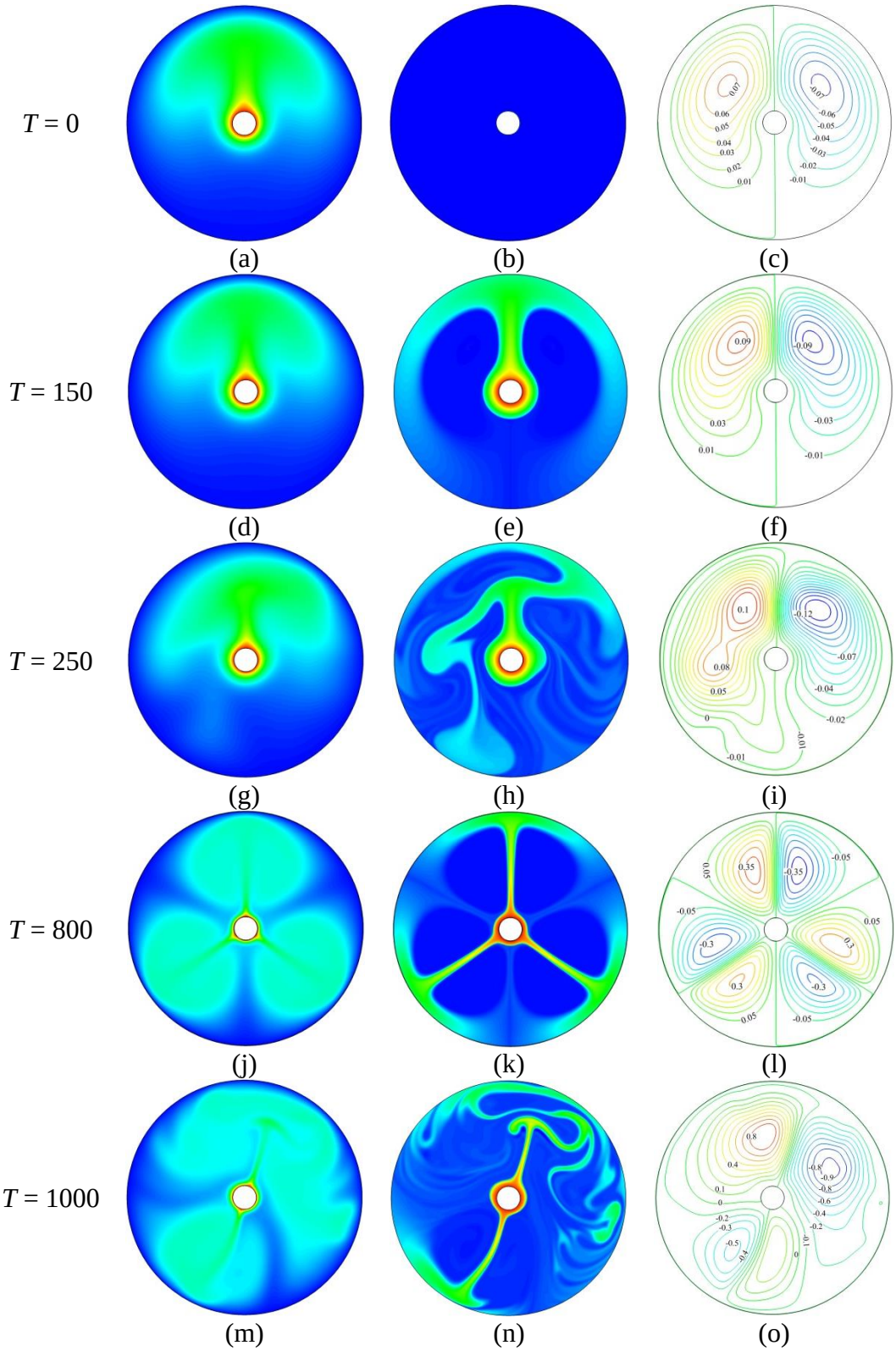

FIG.8. Solutions for $Ra = 10^4$, $T = 0$, 150, 250, 800 and 1000. (a, d, g, j, m) - temperature; (b, e, h, k, n) - charge density; (c, f, i, l, o) - stream function.

A slight increase of Ra to 10^2 puts off the corresponding T_t to be about 75.0. In addition, a new flow pattern appears once $T > T_t$. As shown in Figs. 7a-c, there are two pairs of radial cells and two big charge void regions. The appearance of such a new flow pattern can be understood from the point of view of linear stability. For pure electro-convection the critical values of T corresponding to the 2- and 3-cells modes are very close to each other. That means for T slightly higher than T_c both modes tend to be excited. In the electro-thermal case the initial natural convection helps exciting mode $m = 2$ to be dominant. For $T \geq 250$, the three-pair flow pattern appears again; see Figs. 7d-f. For a high value of T, a strong radial motion is induced by the Coulomb force; see the maximum value of stream function in Fig. 7f. Consequently, the temperature distribution shown in Fig. 7d is mainly determined by the radial convection. There is a transition phase, during which the two-pair and three-pair patterns appear alternatively. This transition phase explains the inflection point at $T = 200$ (between points B and C) in Fig. 5a.

For $Ra \geq 1\times10^3$, the buoyancy force is no longer negligible, at least when T is not very high. In Fig. 8, we have provided the example of $Ra = 10^4$ to show the effects of T on the flow pattern and the distributions of charge density and temperature. The value of T_t for the case of $Ra = 10^4$ is about 225.0. For $T < T_t$, the flow motion is still stationary and shows the same structure as the natural convection (see Figs. 8c and 8f). However, the newly injected charges now move along mainly with the buoyancy force induced motion, since the ion drift velocity $T\vec{E}/M^2$ is much smaller than the fluid velocity $\vec{U}$. Consequently, as shown in Fig. 8e, the charge density shows a plume-like structure at the top region of the annulus. The Coulomb force exerting on these charges fails to induce the radial motion. Instead, it strengthens the velocity filed of natural convection, which can be inferred from the maximum values of stream function and the center

position of rotation in Figs. 8c and 8f. The enhanced flow field explains the slow increase of $\overline{Nu}$ with T in the range of $T < T_t$.

Once $T > T_c$, radial motion arises again. However, the flow is no longer stationary when T is slightly higher than T_t. This is different from the cases of small Ra values discussed above. In addition, the flow pattern is very complex. Three basic patterns including the two big cells associated with natural convection, the two-pair and three-pair patterns with electro-convection interact with each other and appear alternately. The frequency for each basic pattern is very sensitive to the values of Ra and T. In general, the two big-cell pattern dominates when T is closer to T_t and Ra is higher, while the three-pair pattern appears more frequently with T much higher than T_t. Figs. 8g-i represent a snapshot of the unsteady two big-cell pattern at $T = 250$. For $Ra = 5\times10^3$ and 1×10^4, we find that the steady three-pair pattern emerges when T is far from T_t to a certain extent. In Fig. 5b, the transitions at (250, 300) with the curve of $Ra = 5\times10^3$ and at (300, 350) with the curve of $Ra = 1\times10^4$ is due to the appearance of the steady three-pair pattern. Figs. 8j-l show the steady three-pair pattern with $T = 800$. For $Ra = 10^3$, 5×10^3 and 1×10^4, the flow becomes unsteady again with T at 900, which results in a sudden decrease of $\overline{Nu}$; see Fig. 5b. As a matter of fact, the flow becomes fully chaotic and is accompanied with appearance of a new type of electro-plumes; see Fig. 8n. This type of electro-plume, which is a local structure of charges, is randomly and intermittently generated within the charge density layer near the emitter electrode. Such electro-plume shares strong analogy with the thermal plume of Rayleigh-Bénard convection at high Ra values [56], and it has been numerically observed in the configurations of plate-plate [57] and concentric cylinders [58]. It is interesting to point out that there is also a new type of thermal plume in Fig. 8m with its shape and position the same as the electro-plume in Fig. 8n. This is an intuitive example demonstrating that heat is entrained as a fully passive scalar by

the motion induced by charge injection. For $Ra = 1.5\times10^4$ and 2.0×10^4, we did not observed any stationary pattern with $T > T_t$. For these two Ra values, the increase of $\overline{Nu}$ with T is due to the raising portion of the three-pair pattern and the increase of the intensity of convection with T.

Another interesting finding is the independence of $\overline{Nu}$ on Ra when T is high enough and the flow pattern is the same. For example, for T = 800 and $Ra \le 10^4$, the flow pattern is stationary with three-pair cells and $\overline{Nu}$ always takes a value around 5.25; see Figs. 5a and 5b. For another example, for T = 1000 and $10^3 \le Ra \le 2\times10^4$, the flow pattern is chaotic with electro-plumes and the corresponding $\overline{Nu}$ takes a value around 5.29. We attribute this phenomenon to the dominating role played by the Coulomb force while the buoyancy force is globally unimportant. This phenomena has also been observed in the previous experimental [46, 47] and numerical [35, 36] studies with the plate-plate configuration.

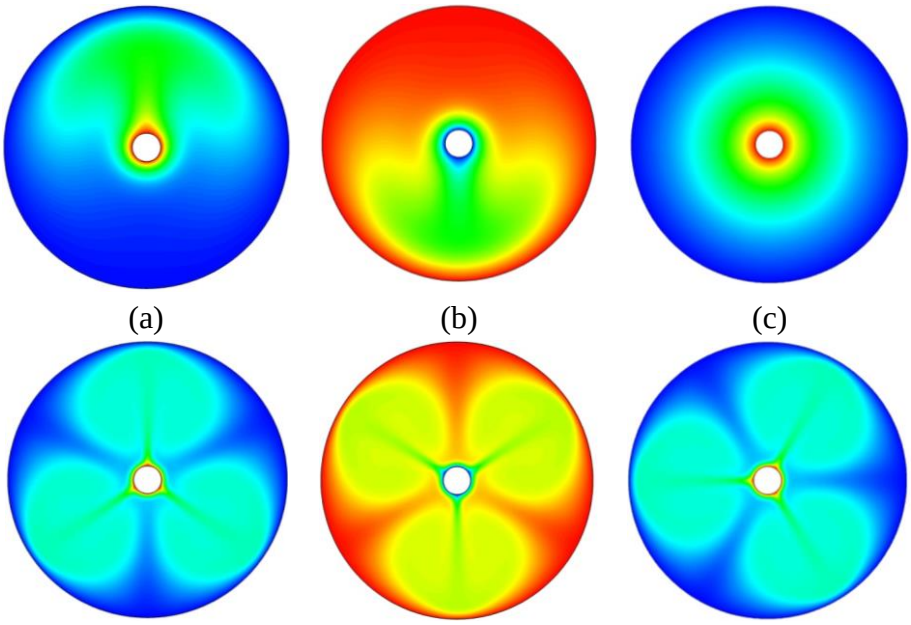

FIG.9. Temperature fields in the annulus without (up) and with (bottom) electric field, (a) and (d), case 1- inner heating; (b) and (e), case 2-outer heating; (c) and (f), case 3-inner heating with zero buoyancy force. Parameters: $Ra = 10^4$ and T = 800.

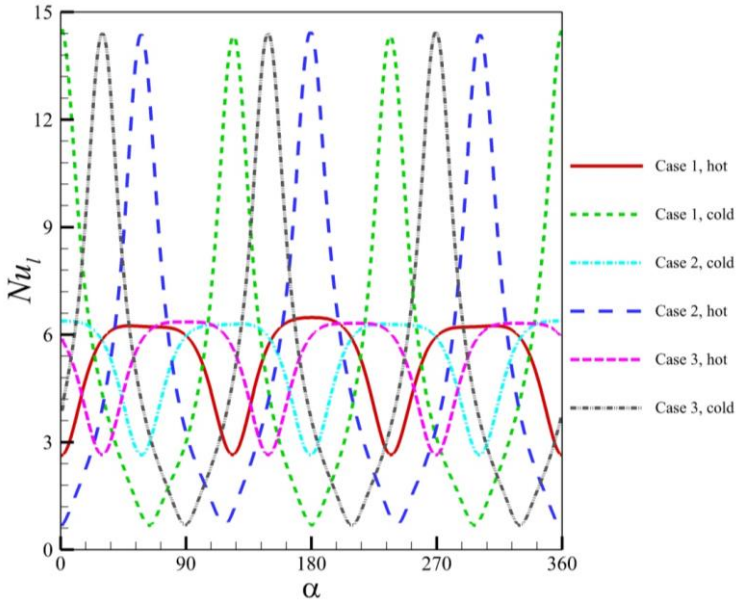

FIG.10. Local Nusselt number distribution after the imposition of electric field and charge injection. Case 1 - inner heating; Case 2 - outer heating; Case 3 – inner heating with zero buoyancy force. Parameters: $Ra = 10^4$ and $T = 800$.

To confirm our understanding of this independence of $\overline{Nu}$ on *Ra*, we have designed a numerical experiment test. Our idea is to check the sensitivity of the flow pattern and $\overline{Nu}$ on the direction and strength of the buoyancy force. For a same *Ra* value, we consider three different situations: (i) heating from the inner cylinder, (ii) heating from the outer cylinder and (iii) heating from inner but with an artificial zero buoyancy force in the Naviers-Stokes equations. The third situation physically corresponds to a microgravity situation, and it can be easily achieved in the numerical practice. Figs. 9a-c show the temperature fields with $Ra = 10^4$ in these three situations with no electric field. Fig. 9c is essentially determined by pure thermal conduction. After imposing the same electric field at $T = 800$, all three situations reach a steadily convective state with three-pair cells. Figs. 9d-f show the temperature fields after the imposition of electric field and charge injection. A quantitative comparison can be made from Fig. 10, in which we have presented the local Nusselt number distributions. It is clearly show that in all cases the maximum

Nu on the inner and outer cylinders are very close to each other. The mean Nusselts numbers for the three cases with electric field are 5.258 (case 1), 5.265 (case 2) and 5.275 (case 3), respectively. These results have successfully proved that the results of $\overline{Nu}$ are independent on the direction and strength of the buoyancy force. That is, the flow is fully dominated by the Coulomb force.

5. Concluding remarks

The enhancement of natural convection heat transfer in a dielectric liquid lying between two concentric horizontal cylinders due to the imposition of a direct current electric field is numerically investigated. The Coulomb force severs as the driving electrical force, and the unipolar injection of ions is considered as the source for free space charges. An in-house numerical solver based on a 2nd finite volume method is developed to solve all governing equations including the mass conservation equation, the Navier-Stokes equations, the energy equation, the charge density transport equation and Gauss' law for the electric field. Computations are carried out for a small radius ratio and a strong injection from the inner cylinder. The silicon oil used in some previous experimental studies is chosen as the working liquid. The heat transfer results expressed through the mean Nusselt numbers $\overline{Nu}$ are presented for the laminar natural convection with $Ra \le 2\times10^4$ and a wide range of the electric driving parameter *T*. It is shown that the injection induced radial convection can yield significant enhancement of heat transfer. The most important finding is the existence of a threshold of *T*, which separates the $\overline{Nu}-T$ curve into two sections. Below this threshold, the radial motion does not arise and $\overline{Nu}$ only slightly increases with *T*. Once *T* is higher than the threshold value, the radial motion with more convective cells takes place and $\overline{Nu}$ rapidly increases with *T*. This threshold value increases with *Ra*. For small *Ra* values, it tends to its lower limit, the linear

stability criterion of pure electro-convection. In addition, the electrical enhancement is found to be closely related to the flow patterns and the values of *Ra* and *T*. Furthermore, for sufficiently high values of *T*, the convective heat transfer no longer depends on *Ra* in the range of parameters considered. This can be understood by the dominant role played by the Coulomb force while the buoyancy force is unimportant.

In a future work, we will perform a systematic study of the effects of various parameters and different injection models on heat transfer. In particular, the influence of the dimensionless mobility number and Prandlt number on the local and mean heat transfer will be evaluated, since the result may be helpful in selecting the optimal working liquid.

Acknowledgements

This work was funded by the French Government program “Investissements d’Avenir” (LABEX INTERACTIFS, reference ANR-11-LABX-0017-01) (to Jian Wu), a grant from the French district Poitou–Charentes (to P. Traoré) and financial support from the Spanish Ministerio de Cienciay Tecnología (MCYT) under Research Project No. FIS2011-25161 and Junta de Andalucía under research projects P10-FQM-5735 and P09-FQM-4584 (to A. T. Pérez).

References

[1] Jones, T. B. (1978). Electrohydrodynamically enhanced heat transfer in liquids - A review. *Advances in heat transfer*, 14, 107-148.

[2] Castellanos, A. (Ed.). (1998). Electrohydrodynamics (No. 380). Springer Science & Business Media.

[3] Seyed-Yagoobi, J., & Bryan, J. E. (1999). Enhancement of heat transfer and mass transport in single-phase and two-phase flows with electrohydrodynamics. *Advances in heat transfer*, 33, 95-186.

[4] Senftleben, H., & Braun, W. (1936). Der Einfluss elektrischer Felder auf den Wärmestrom in Gasen. *Zeitschrift für Physik*, *102*(7-8), 480-506.

[5] Ahsmann, G., & Kronig, R. (1951). The influence of electric fields on the convective heat transfer in liquids. *Applied Scientific Research*, *2*(1), 235-244.

[6] De Haan, H. J. (1951). The influence of electric fields on the convective heat transfer in liquids II. *Applied Scientific Research, Section A*, *3*(1), 85-88.

[7] Vatan, S. N., Nia, E. S., & Merdasi, A. (2014). Empirical correlation for performance evaluation of electric/corona wind on natural convection. *Journal of Electrostatics*, *72*(1), 82-90.

[8] Go, D. B., Garimella, S. V., Fisher, T. S., & Mongia, R. K. (2007). Ionic winds for locally enhanced cooling. *Journal of Applied Physics*, 102(5), 053302.

[9] Yazdani, M., & Seyed-Yagoobi, J. (2010). Heat transfer augmentation of parallel flows by means of electric conduction phenomenon in macro-and microscales. *Journal of Heat Transfer*, 132(6), 062402.

[10] Grassi, W., Testi, D., & Saputelli, M. (2005). EHD enhanced heat transfer in a vertical annulus. *International Communications in Heat and Mass Transfer*, 32(6), 748-757.

[11] Grassi, W., & Testi, D. (2006). Heat transfer enhancement by electric fields in several heat exchange regimes. *Annals of the New York Academy of Sciences*, 1077(1), 527-569.

[12] Laohalertdecha, S., Naphon, P., & Wongwises, S. (2007). A review of electrohydrodynamic enhancement of heat transfer. *Renewable and Sustainable Energy Reviews*, 11(5), 858-876.

[13] Léal, L., Miscevic, M., Lavieille, et al. (2013). An overview of heat transfer enhancement methods and new perspectives: Focus on active methods using electroactive materials. *International Journal of Heat and Mass Transfer*, 61, 505-524.

[14] Atten, P. (1996). Electrohydrodynamic instability and motion induced by injected space charge in insulating liquids. *IEEE Transactions on Dielectrics and Electrical Insulation*, 3(1), 1-17.

[15] Worraker, W. J., & Richardson, A. T. (1979). The effect of temperature-induced variations in charge carrier mobility on a stationary electrohydrodynamic instability. *Journal of Fluid Mechanics*, *93*(01), 29-45.

[16] Takashima, M., & Hamabata, H. (1984). The stability of natural convection in a vertical layer of dielectric fluid in the presence of a horizontal ac electric field. *Journal of the Physical Society of Japan*, 53(5), 1728-1736.

[17] Smorodin, B. L., & Velarde, M. G. (2001). On the parametric excitation of electrothermal instability in a dielectric liquid layer using an alternating electric field. *Journal of Electrostatics*, 50(3), 205-226.

[18] Shivakumara, I. S., Lee, J., Vajravelu, K., & Akkanagamma, M. (2012). Electrothermal convection in a rotating dielectric fluid layer: Effect of velocity and temperature boundary conditions. *International Journal of Heat and Mass Transfer*, *55*(11), 2984-2991.

[19] Malik, S. V., Yoshikawa, H. N., Crumeyrolle, O., & Mutabazi, I. (2012). Thermo-electro-hydrodynamic instabilities in a dielectric liquid under microgravity. *Acta Astronautica*, 81(2), 563-569.

[20] Yoshikawa, H. N., Crumeyrolle, O., & Mutabazi, I. (2013). Dielectrophoretic force-driven thermal convection in annular geometry. *Physics of Fluids*, *25*(2), 024106.

[21] Castellanos, A. (1991). Coulomb-driven convection in electrohydrodynamics. *IEEE Transactions on Electrical Insulation*, 26(6), 1201-1215.

[22] Martin, P. J., & Richardson, A. T. (1984). Conductivity models of electrothermal convection in a plane layer of dielectric liquid. *Journal of heat transfer*, 106(1), 131-136.

[23] Chang, M. H., Ruo, A. C., & Chen, F. (2009). Electrohydrodynamic instability in a horizontal fluid layer with electrical conductivity gradient subject to a weak shear flow. *Journal of Fluid Mechanics*, 634, 191-215.

[24] Ding, Z., & Wong, T. N. (2014). Electrohydrodynamic instability in an annular liquid layer with radial conductivity gradients. *Physical Review E*, *89*(3), 033010.

[25] Lacroix, J. C., Atten, P., & Hopfinger, E. J. (1975). Electro-convection in a dielectric liquid layer subjected to unipolar injection. *Journal of Fluid Mechanics*, 69(03), 539-563.

[26] Malraison, B., & Atten, P. (1982). Chaotic behavior of instability due to unipolar ion injection in a dielectric liquid. *Physical Review Letters*, 49(10), 723.

[27] Pontiga, F., & Castellanos, A. (1994). Physical mechanisms of instability in a liquid layer subjected to an electric field and a thermal gradient. *Physics of Fluids*, 6(5), 1684-1701.

[28] Pontiga, F., & Castellanos, A. (1996). The effect of field-enhanced injection and dissociation on the conduction of highly-insulating liquids. *IEEE Transactions on Dielectrics and Electrical Insulation*, 3(6), 792-799.

[29] Pontiga, F., & Castellanos, A. (1997). A dissociation-injection model for non-polar liquid conduction and wire-cylinder geometry. *IEEE Transactions on Dielectrics and Electrical Insulation*, 4(2), 224-237.

[30] Denat, A., Gosse, B., & Gosse, J. P. (1979). Ion injections in hydrocarbons. *Journal of Electrostatics*, 7, 205-225.

[31] Alj, A., Denat, A., Gosse, J. P., Gosse, B., & Nakamura, I. (1985). Creation of charge carriers in nonpolar liquids. *IEEE Transactions on Electrical Insulation*, 2, 221-231.

[32] Suh, Y. K. (2012). Modeling and simulation of ion transport in dielectric liquids-Fundamentals and review. *IEEE Transactions on Dielectrics and Electrical Insulation*, 19(3), 831-848.

[33] Fernández, J., & Poulter, R. (1987). Radial mass flow in electrohydrodynamically-enhanced forced heat transfer in tubes. *International Journal of Heat and Mass Transfer, 30(10)*, 2125-2136.

[34] Grigsby, L. L., et al. (2001). The Electric Power Engineering Handbook. USA: CRC Press.

[35] Traoré, P., Pérez, A. T., Koulova, D., & Romat, H. (2010). Numerical modelling of finite-amplitude electro-thermo-convection in a dielectric liquid layer subjected to both unipolar injection and temperature gradient. *Journal of Fluid Mechanics, 658*, 279-293.

[36] Wu, J., & Traoré, P. (2015). A Finite-Volume method for electro-thermo-convective phenomena in a plane layer of dielectric liquid. *Numerical Heat Transfer, Part A: Applications*, 68(5), 471-500.

[37] Wu, J., Vázquez, P. A., Traoré, P., & Pérez, A. T. (2014). Finite amplitude electroconvection induced by strong unipolar injection between two coaxial cylinders. *Physics of Fluids*, 26(12), 124105.

[38] Pérez, A. T., & Castellanos, A. (1989). Role of charge diffusion in finite-amplitude electroconvection. *Physical Review A*, 40(10), 5844.

[39] Ferziger, J. H., & Perić, M. (2002). *Computational methods for fluid dynamics*. Berlin: Springer.

[40] Jasak, H. (1996). Error analysis and estimation for the finite volume method with applications to fluid flows, *Ph.D. Thesis*, Imperial College, University of London, 83-86.

[41] Demirdžić, I. (2015). On the Discretization of the Diffusion Term in Finite-Volume Continuum Mechanics. *Numerical Heat Transfer, Part B: Fundamentals*, *68*(1), 1-10.

[42] Patankar, S. V., & Spalding, D. B. (1972). A calculation procedure for heat, mass and momentum transfer in three-dimensional parabolic flows. *International Journal of Heat and Mass Transfer*, 15(10), 1787-1806.

[43] Rhie, C. M., & Chow, W. L. (1983). Numerical study of the turbulent flow past an airfoil with trailing edge separation. *AIAA journal*, 21(11), 1525-1532.

[44] Wu, J., Traoré, P., & Louste, C. (2013). An efficient finite volume method for electric field–space charge coupled problems. *Journal of Electrostatics*,71(3), 319-325.

[45] Gaskell, P. H., & Lau, A. K. C. (1988). Curvature - compensated convective transport: SMART, A new boundedness - preserving transport algorithm. *International Journal for Numerical Methods in Fluids*, 8(6), 617-641.

[46] Atten, P., McCluskey, F. M. J., & Pérez, A. T. (1988). Electroconvection and its effect on heat transfer. *IEEE Transactions on Electrical Insulation*, 23(4), 659-667.

[47] McCluskey, F. M. J., Atten, P., & Pérez, A. T. (1991). Heat transfer enhancement by electroconvection resulting from an injected space charge between parallel plates. *International Journal of Heat and Mass Transfer*, 34(9), 2237-2250.

[48] Kuehn, T. H., & Goldstein, R. J. (1976). An experimental and theoretical study of natural convection in the annulus between horizontal concentric cylinders. *Journal of Fluid Mechanics*, 74(04), 695-719.

[49] Teertstra, P., & Yovanovich, M. M. (1998). Comprehensive review of natural convection in horizontal circular annuli. *ASME-PUBLICATIONS-HTD*, 357, 141-152.

[50] Angeli, D., Barozzi, G. S., Collins, M. W., & Kamiyo, O. M. (2010). A critical review of buoyancy-induced flow transitions in horizontal annuli. *International Journal of Thermal Sciences*, 49(12), 2231-2241.

[51] Yan-Fei, R., Yasutomi, M., Kenji, F., Yasuyuki, T., & Shu, H. (1985). Flow patterns of natural convection in horizontal cylindrical annuli. *International Journal of Heat and Mass Transfer*, 28(3), 705-714.

[52] Agrät, N., & Castellanos, A. (1990). Linear convective patterns in cylindrical geometry for unipolar injection. *Physics of Fluids A: Fluid Dynamics (1989-1993)*, 2(1), 37-44.

[53] Richardson, A. T., & Poulter, R. (1976). Electrophoretic instability in a diffusion-free dielectric liquid in an annular geometry. *Journal of Physics D: Applied Physics*, 9(4), L45.

[54] Richardson, A. T. (1980). The linear instability of a dielectric liquid contained in a cylindrical annulus and subjected to unipolar charge injection. *The Quarterly Journal of Mechanics and Applied Mathematics*, 33(3), 277-292.

[55] Fernandes, D. V., Lee, H. D., Park, S., & Suh, Y. K. (2013). Electrohydrodynamic instability of dielectric liquid between concentric circular cylinders subjected to unipolar charge injection. *Journal of Mechanical Science and Technology*, 27(2), 461-467.

[56] Lohse, D., & Xia, K. Q. (2010). Small-scale properties of turbulent Rayleigh-Bénard convection. *Annual Review of Fluid Mechanics*, 42, 335-364.

[57] Traoré, P., & Pérez, A. T. (2012). Two-dimensional numerical analysis of electroconvection in a dielectric liquid subjected to strong unipolar injection. *Physics of Fluids*, 24(3), 037102.

[58] Fernandes, D. V., Lee, H. D., Alapati, S., & Suh, Y. K. (2012). Numerical simulation of the electro-convective onset and complex flows of dielectric liquid in an annulus. *Journal of Mechanical Science and Technology*, 26(12), 3785-3793.